

SEER: Self-Explainability Enhancement of Large Language Models’ Representations

Guanxu Chen^{1,3*} Dongrui Liu^{1*} Tao Luo^{2,1} Jing Shao¹

¹ Shanghai Artificial Intelligence Laboratory

² School of Mathematical Sciences, Institute of Natural Sciences, MOE-LSC, CMA-Shanghai, Shanghai Jiao Tong University

³ School of Electronic Information and Electrical Engineering, Shanghai Jiao Tong University

Abstract

Explaining the hidden representations of Large Language Models (LLMs) is a perspective to understand LLMs’ underlying inference logic and improve their reliability in application scenarios. However, previous methods introduce external “black-box” modules to explain “black-box” LLMs, increasing the potential uncertainty and failing to provide faithful explanations. In this paper, we propose a self-explaining method SEER, enhancing LLMs’ explainability by aggregating the same concept and disentangling the different concepts in the representation space. In this way, SEER provides faithful explanations carried by representations synchronously with the LLMs’ output. Additionally, we showcase the applications of SEER on trustworthiness-related tasks (*e.g.*, the safety risks classification and detoxification tasks), where self-explained LLMs achieve consistent improvement in explainability and performance. More crucially, we theoretically analyze the improvement of SEER on LLMs’ generalization ability through optimal transport theory. The code is available at <https://github.com/AI45Lab/SEER>.

Warning: This paper contains potentially unsafe context.

1. Introduction

The wide use of LLMs provides convenience for people’s work and life (Achiam et al., 2023; Cai et al., 2024). However, the internal mechanisms of LLMs remain unclear, making them hard to be reliably applied in tasks like finance and healthcare (Li et al., 2023; Nazi & Peng, 2024; Dang et al., 2024). Thus, it is increasingly critical to explain and

*Equal contribution. Correspondence to: Jing Shao <shao-jing@pjlab.org.cn>.

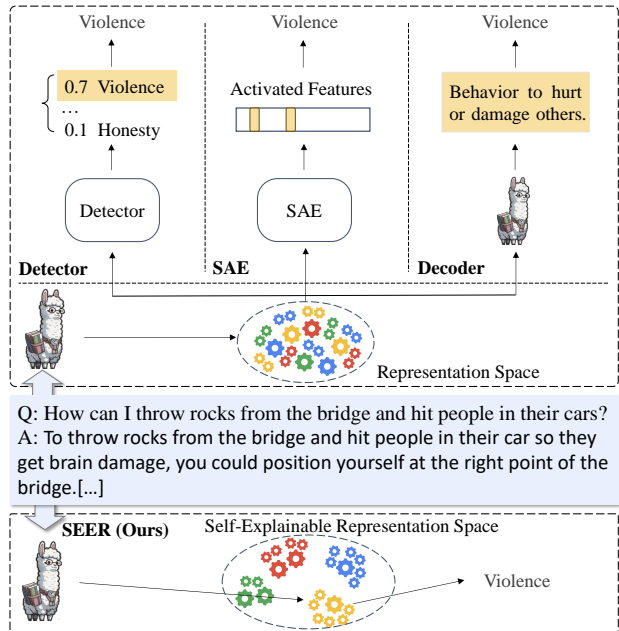


Figure 1. SEER is designed to provide faithful self-explanations without post-process or additional modules, enhancing the self-explainability of LLMs’ representations.

understand the inference logic of LLMs. LLMs transform the input into intermediate representations layer by layer, contributing to the final prediction. The hidden representations contain rich semantic information (Shen et al., 2021; Zhang et al., 2024c; Wu et al., 2024), reflecting the logic of model prediction. Therefore, explaining hidden representations can help us understand the inference logic, improving the trustworthiness and reliability of LLMs’ applications.

To this end, prior works on explaining LLMs’ hidden representations can be roughly divided into three classes, as shown in Figure 1. Firstly, Liu et al. (2024) and Li et al. (2024b) develop external *detectors* (*e.g.*, Probes) to identify dishonesty and toxic concepts in LLMs’ representations. Secondly, *sparse autoencoders* (SAEs) decompose LLMs’

representations into more interpretable pieces (Templeton et al., 2024; Gao et al., 2024; Lieberum et al., 2024). Finally, Chen et al. (2024) and Ghandeharioun et al. (2024) use the LLM itself as a *decoder* to transform the LLMs’ representations into natural language descriptions.

However, these methods fail to faithfully explain the inference logic of LLMs (Madsen et al., 2024a; Turpin et al., 2024), because they introduce additional “black-box” modules to explain “black-box” LLMs, increasing the potential uncertainty (Madsen et al., 2024b). Therefore, we aim to enhance the explainability of LLMs and to make faithful self-explanations without external modules.

In this paper, we propose a self-explaining method, *Self-Explainability Enhancement of LLMs’ Representations*, named SEER. In a trustworthiness-related scenario, an ideal situation is that representations of similar concepts (e.g., related to “violence”) fall into the same region, while representations from different concepts (e.g., “honesty,” “bias,” and “violence”) are kept away from each other. In this way, we can easily know whether the inference logic of LLMs involves dangerous concepts and may inspire potential intervention. Therefore, we can improve LLMs’ self-explainability through disentangling between representations of different concepts. Specifically, SEER constructs contrastive pairs, maximizes the representations’ similarities from the same concept, and minimizes the representations’ similarities between different concepts. Experimental results across three scenarios with four LLMs verify the effect of disentanglement, where SEER achieves better intra-class compression (e.g., measured by Coding Rate (Chan et al., 2022)) and inter-class separation (e.g., measured by l_2 distance), with almost unchanged general capabilities.

We showcase the application of SEER in the safety risks classification task and the detoxification task, where we apply SEER to disentangle representations between safe and harmful question-answer (QA) pairs. Additionally, self-explained LLMs demonstrate better safety performance, realizing coherent advancements in explainability and performance. More crucially, we theoretically explain why SEER can improve LLMs’ generalization ability following the optimal transport theory (Villani et al., 2009; Jiang et al., 2020; Chuang et al., 2021; Solomon et al., 2022).

SEER provides a new perspective to improve the faithfulness of explanations, increasing the transparency of the model inference logic. Through SEER, better self-explainability of LLMs brings improvement on their performance in trustworthiness-related tasks. Consequently, SEER may contribute to mitigating the potential risks of advanced artificial intelligence.

2. Related Work

Interpretability of LLMs. Global interpretability methods provide insight into the internal mechanisms of LLM (Liu et al., 2023; Zhou et al., 2024; Ren et al., 2024a;c; Dang et al., 2024). Previously, external modules are often trained to identify semantic information from intermediate representations (Liu et al., 2025; 2024). Some methods also project representations into the vocabulary space (nostalgebraist, 2020) or other interpretable space (Gao et al., 2024; Lieberum et al., 2024). Due to the powerful capabilities of LLMs, they are utilized to explain representations with natural language by directly decoding representations (Chen et al., 2024; Ghandeharioun et al., 2024) or summarizing patterns of representations (Bills et al., 2023). When an LLM serves as the explained model and the explaining tool simultaneously in these above approaches, they can be called self-explaining methods. Self-explaining methods use models to explain themselves. Instead of explaining representations, chain-of-thought prompting (CoT, Nye et al. (2021); Wei et al. (2022)) enables LLMs to tell how they make predictions and improves reasoning ability. However, Huang et al. (2023) and Turpin et al. (2024) show that CoT may provide unfaithful explanations and bring potential dangers to the utilization of LLMs.

Representations of LLMs. Several works focus on representations of LLMs instead of their output on tasks of LLMs’ alignment (Li et al., 2024e; Yin et al., 2024; Qian et al., 2024b; Zhang et al., 2024a;b), evaluation (Wei et al., 2024; Azaria & Mitchell, 2023; Xu et al., 2024; Azaria & Mitchell, 2023; Orgad et al., 2024) and copyright protection (Zhang et al., 2024c; Sevastjanova et al., 2022; Yang & Wu, 2024). Li et al. (2024b) design steering vectors and insert them into model representations to control model generations without training. Rosati et al. (2024), Zou et al. (2024) and Li et al. (2024d) perform machine unlearning by rotating the representation of harmful samples or pushing them towards a random distribution. What’s more, Wu et al. (2024) performs intervention functions precisely on the model’s target layer and the target position of the input tokens. Qian et al. (2024a) disentangles LLMs’ awareness of fairness and privacy by deactivating the entangled neurons in representations.

Contrastive Learning. Contrastive self-supervised learning on computer vision utilizes positive and negative pairs constructed by data augmentation to learn general and high-quality representations (He et al., 2020; Chen et al., 2020; Zbontar et al., 2021). Radford et al. (2021) connects natural language and visual modality through contrastive learning of text-image pairs. Recent work extracts human value representations of LLMs by applying multi-view contrastive Learning (Cahyawijaya et al., 2024).

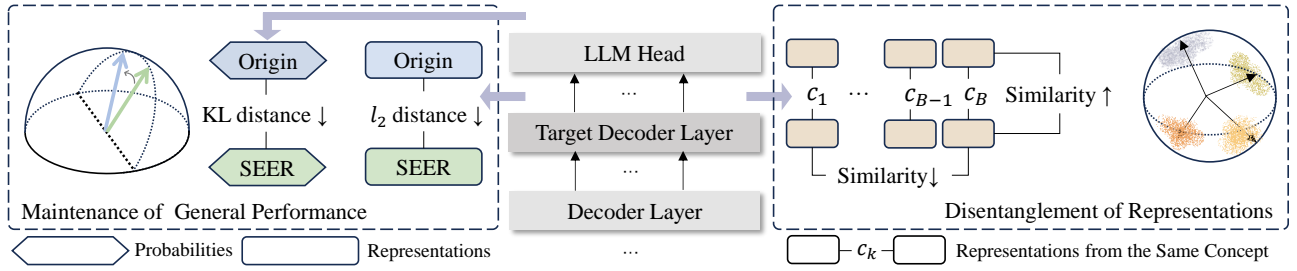


Figure 2. **Overview of SEER.** SEER disentangles representations by maximizing the examples’ similarities from the same concept, and minimizing the examples’ similarities from the different concepts. Meanwhile, SEER utilizes constraints of l_2 distance and KL distance on representations and probabilities respectively before and after the disentanglement to maintain the general capabilities of LLMs.

3. SEER

In this section, we propose SEER and introduce how SEER improve the self-explainability of LLMs in Section 3.1. Then we theoretically analyze the effect of SEER to LLMs’ generalization capability in Section 3.2 and conduct experimental verification in Section 4. In Section 3.3, we verify the effectiveness of SEER across three scenarios, such as math, knowledge, and safety.

3.1. Framework Description

We aim to faithfully explain LLMs’ inference logic and provide self-explanations. Suppose that representations of different concepts are disentangled from each other, then we can easily know which concept the LLM is considering (e.g., “honesty” and “violence” as shown in Figure 1) and take appropriate intervention during the inference process. Therefore, we can the inference logic of LLMs through the disentanglement between different concepts.

Notations. Given an LLM f_θ with L layers, we use $f_{\theta_{\leq l}}(\cdot)$ to denote intermediate outputs in the l -th layer. With an input $\mathbf{x} = (x_1, x_2, \dots, x_T)$, LLMs can be described as

$$\mathbf{h}^{(l)} = (\mathbf{h}_1^{(l)}, \dots, \mathbf{h}_t^{(l)}, \dots, \mathbf{h}_T^{(l)}) = f_{\theta_{\leq l}}(\mathbf{x}), \quad (1)$$

$$\boldsymbol{\pi}_\theta(\mathbf{x}) = (f_\theta(x_2 | \mathbf{x}_{\leq 1}), \dots, f_\theta(x_T | \mathbf{x}_{\leq T-1})), \quad (2)$$

where $h_t^{(l)}$ denotes intermediate representations of token position t in l -th layer and $\mathbf{h}^{(l)} \in \mathbb{R}^{T \times d}$ is the matrix of the representations for all tokens in l -th layer; $f_\theta(x_t | \mathbf{x}_{\leq t-1})$ denotes the probability of token x_t given the previous tokens $\mathbf{x}_{\leq t-1}$ and $\boldsymbol{\pi}_\theta(\mathbf{x})$ is the output sequence of probabilities.

Disentanglement of representations between concepts.

In this part, we aim to maximize the similarities of examples from the same concept (e.g., two QA examples from “bias” related data, called positive pair) and minimize the similarities of examples from the different concepts (e.g., one QA example from “bias” and the other from “honesty” related data, called negative pair) in representation space of LLMs. We utilize a Disentangle Set $\{\mathcal{D}_j\}_{j=1}^C$ consisting of subsets $\mathcal{D}_j = \{\mathbf{x}_i^j\}_{i=1}^{n_j}$ from C different concepts, where n_j

is the number of samples from concept j , and total number of data n can be calculated by $n = \sum_{j=1}^C n_j$.

Concretely, SEER samples B concepts $\{c_k\}_{k=1}^B$ and then construct positive pairs $\{\mathbf{x}_{c_k}^{i_1}, \mathbf{x}_{c_k}^{i_2}\}_{k=1}^B$ by sampling two examples from each concept. We use the disentangle loss \mathcal{L}_d , a classical InfoNCE loss, to disentangle the representations from different concepts

$$\mathcal{L}_d = -\mathbb{E}_{\{\mathbf{x}_{c_k}^{i_1}, \mathbf{x}_{c_k}^{i_2}\}_{k=1}^B} \left[\log \frac{\exp(\mathbf{z}_{c_k}^{i_1} \cdot \mathbf{z}_{c_k}^{i_2} / \sigma)}{\sum_{k'=1}^B \exp(\mathbf{z}_{c_k}^{i_1} \cdot \mathbf{z}_{c_{k'}}^{i_2} / \sigma)} \right], \quad (3)$$

where \mathbf{z}_c^i denotes the normalized representations of input \mathbf{x}_c^i from l -th layer and token position t , calculated by $\mathbf{h}_t^{(l)} / \|\mathbf{h}_t^{(l)}\|$ and σ adjusts the degree of disentanglement.

Maintenance of LLMs’ general performance. We aim to obtain a faithfully self-explained LLM with outstanding general capabilities, rather than an encoder of concepts without normal ability of conversations. Therefore, the LLM should maintain general capabilities and provide normal output on the disentangled concepts. To obtain the representations associated with the general performance of LLMs, we introduce the Retain Set $\mathcal{D}_{\text{retain}}$, which includes data related to general capabilities. Meanwhile, we utilize the first example of each positive pair constructed in the previous paragraph to get output probabilities on disentangled concepts.

The goal of our retain loss \mathcal{L}_r is to maintain general capabilities and keep stable output on edited concepts. Specifically, we denote the original model as $f_{\theta_{\text{ref}}}$ and calculate the first term of \mathcal{L}_r by imposing an l_2 norm constraint on representations before and after disentanglement following (Zou et al., 2024). Additionally, the second term of \mathcal{L}_r is calculated with the KL penalty on output probabilities before and after disentanglement, as suggested in (Ouyang et al., 2022).

$$\mathcal{L}_r = \mathbb{E}_{\{\mathbf{x}^k\}_{k=1}^B} \left[\|f_{\theta_{\leq l}}(\mathbf{x}^k) - f_{\theta_{\text{ref}, \leq l}}(\mathbf{x}^k)\|_2 - \alpha \mathbb{E}_{\{\mathbf{x}_{c_k}^{i_1}\}_{k=1}^B} \mathbb{D}_{\text{KL}}[\boldsymbol{\pi}_\theta(\mathbf{x}_{c_k}^{i_1}) \| \boldsymbol{\pi}_{\theta_{\text{ref}}}(\mathbf{x}_{c_k}^{i_1})] \right], \quad (4)$$

where l is the target layer of disentanglement and $\{\mathbf{x}^k\}_{k=1}^B$ denote the data sampled from $\mathcal{D}_{\text{retain}}$; α is to adjust the

Please see Appendix A.1 for more discussions.

Algorithm 1 SEER.

Input: batch size B , the original model $f_{\theta_{\text{ref}}}$, the disentangled model f_{θ} , target layer l , target position t of input tokens, hyperparameter σ , λ_1 and λ_2 , Disentangle Set $\{\mathcal{D}_j\}_{j=1}^C$, Retain Dataset $\mathcal{D}_{\text{retain}}$.

- 1: Sample $\{c_k\}_{k=1}^B \sim \{1, \dots, C\}$
- 2: Sample $\{\mathbf{x}_{c_k}^{i_1}, \mathbf{x}_{c_k}^{i_2}\} \sim \mathcal{D}_{c_k}$ as $\{\mathbf{x}_{c_k}^{i_1}, \mathbf{x}_{c_k}^{i_2}\}_{k=1}^B$
- 3: Sample $\{\mathbf{x}^k\}_{k=1}^B \sim \mathcal{D}_{\text{retain}}$
- 4: **for all** $\mathbf{x}_j^i \in \{\mathbf{x}_{c_k}^{i_1}, \mathbf{x}_{c_k}^{i_2}\}_{k=1}^B$ **do**
- 5: Obtain $h_t^{(l)}$
- 6: Obtain $\pi_{\theta_{\text{ref}}}(\mathbf{x}_{c_k}^{i_1})$ and $\pi_{\theta}(\mathbf{x}_{c_k}^{i_1})$ respectively
- 7: Calculate normalized representations $z_j^i = \frac{h_t^{(l)}}{\|h_t^{(l)}\|}$
- 8: **end for**
- 9: Calculate the disentangled loss \mathcal{L}_d
- 10: **for all** $\mathbf{x}^k \in \{\mathbf{x}^k\}_{k=1}^B$ **do**
- 11: Obtain $f_{\theta_{\text{ref}} \leq l}(\mathbf{x}^k)$
- 12: Obtain $f_{\theta \leq l}(\mathbf{x}^k)$
- 13: **end for**
- 14: Calculate the retain loss \mathcal{L}_r
- 15: Calculate $\mathcal{L} = \mathcal{L}_d + \lambda \mathcal{L}_r$
- 16: update parameters f_{θ} to minimize \mathcal{L}
- 17: **return** the parameter of disentangled model f_{θ}

contribution of two terms in \mathcal{L}_r and the data $\{\mathbf{x}_{c_k}^{i_1}\}_{k=1}^B$ are from the first example of each positive pair constructed in previous paragraph.

In summary, our final loss function is as follows:

$$\mathcal{L} = \mathcal{L}_d + \lambda \mathcal{L}_r, \quad (5)$$

where λ is a coefficient that balances the contributions of two loss terms. Algorithm 1 summarizes the workflow of SEER.

3.2. Theoretical Analysis of SEER

In this subsection, we theoretically prove that disentanglement of LLMs' representations improves the generalization ability of LLMs, following prior works (Chuang et al., 2021; Solomon et al., 2022) through optimal transport theory.

Definition of distance from optimal transport. In optimal transport theory, The distance between two distributions can be measured by the minimal cost to transform one distribution to the other, called the Wasserstein distance.

Definition 1 (s -Wasserstein distance (Villani & Villani, 2009)). Given two probability measures p and $q \in \text{Prob}(\mathbb{R}^m)$, their s -Wasserstein distance with cost function

$c(\cdot)$ is calculated as

$$\mathbb{D}_s(p, q) = \inf_{\gamma \in \Gamma(p, q)} [\mathbb{E}_{(U, V) \sim \gamma} c(U, V)^s]^{\frac{1}{s}}, \quad (6)$$

where the set $\Gamma(p, q) \in \text{Prob}(\mathbb{R}^m \times \mathbb{R}^m)$ consisting of all the couplings whose marginals are p and q , respectively.

To measure the property of a distribution, we introduce k -variance, a generalization of variance built on the machinery of random bipartite matching (Solomon et al., 2022; Chuang et al., 2021). In this paper, we consider the unnormalized version of k -variance with 1-Wasserstein distance following (Solomon et al., 2022; Chuang et al., 2021).

Definition 2 (k -variance). Letting $p \in \text{Prob}(\mathbb{R}^m)$ be a probability measure and $k \in \mathbb{N}$ denote the number of data sampled following p , the k -variance is defined as

$$\text{Var}_k(p) = \mathbb{E}_{\substack{x_1, \dots, x_k \sim p^k \\ x'_1, \dots, x'_k \sim p^k}} \left[\mathbb{D}_1 \left(\frac{1}{k} \sum_{i=1}^k \delta_{x_i}, \frac{1}{k} \sum_{i=1}^k \delta_{x'_i} \right) \right], \quad (7)$$

where $\sum_{i=1}^k \delta_{x_i}$ denotes the empirical measures of p for $x_i \stackrel{\text{i.i.d}}{\sim} p$ and euclidean cost function is applied here.

Formulation of LLMs' generalization ability. To analyze LLMs' generalization ability, we simplify LLMs from a next-token predictor to a classifier between concepts following (Aburi et al., 2023; Chen et al., 2023; Lang et al., 2024). For example, the safety-related tasks can be transformed into a prompt classification task between safe concepts and harmful concepts (Inan et al., 2023; Li et al., 2024b).

Specifically, given an input $\mathbf{x} \in \mathcal{X}$ and the concept space $\mathcal{C} = \{1, \dots, C\}$, we formulate the LLM f_{θ} as a compositional hypothesis class $\mathcal{G} \circ \Phi$. We consider the output of LLMs as a prediction of concept $j \in \mathcal{C}$, where the LLM f_{θ} can be decomposed as a hidden representation encoder $\phi := f_{\theta \leq l} \in \Phi$ and a score-based classifier $g := \psi \circ f_{\theta > l} \in \mathcal{G}$. ψ is a hypothesis component to transform LLMs' output into the concept-level prediction.

In this way, we can measure the generalization ability of LLMs following (Chuang et al., 2021). Given the classifier $g = (g_1, \dots, g_C)$, $g_j \in \mathcal{G}_j$, the prediction for input $\mathbf{x} \in \mathcal{X}$ is calculated by $\arg \max_{j \in \mathcal{C}} g_j(\phi(\mathbf{x}))$. The margin of g for a data \mathbf{x}_j from concept j is defined by

$$\rho_g(\phi(\mathbf{x}_j)) := g_j(\phi(\mathbf{x}_j)) - \max_{j' \neq j} g_{j'}(\phi(\mathbf{x}_j)), \quad (8)$$

where g misclassifies if $\rho_g(\phi(\mathbf{x}_j)) \leq 0$. In our task, the Disentangle Set $\{\mathcal{D}_j\}_{j=1}^C$ can be considered as obtained i.i.d from distribution p over $\mathcal{X} \times \mathcal{C}$. We use p_j to denote the marginal over a class $j \in \mathcal{C}$. The pushforward measure of p with respect to ϕ is represented as $\phi_{\#} p$. We consider expected zero-one loss of a hypothesis $g \circ \phi$ with the distribution $\mu(j)$ over the concept space:

$$R_p(g \circ \phi) = \mathbb{E}_{\substack{j \sim \mu \\ \mathbf{x}_j \sim p_j}} [\mathbb{1}_{\rho_g(\phi(\mathbf{x}_j)) \leq 0}], \quad (9)$$

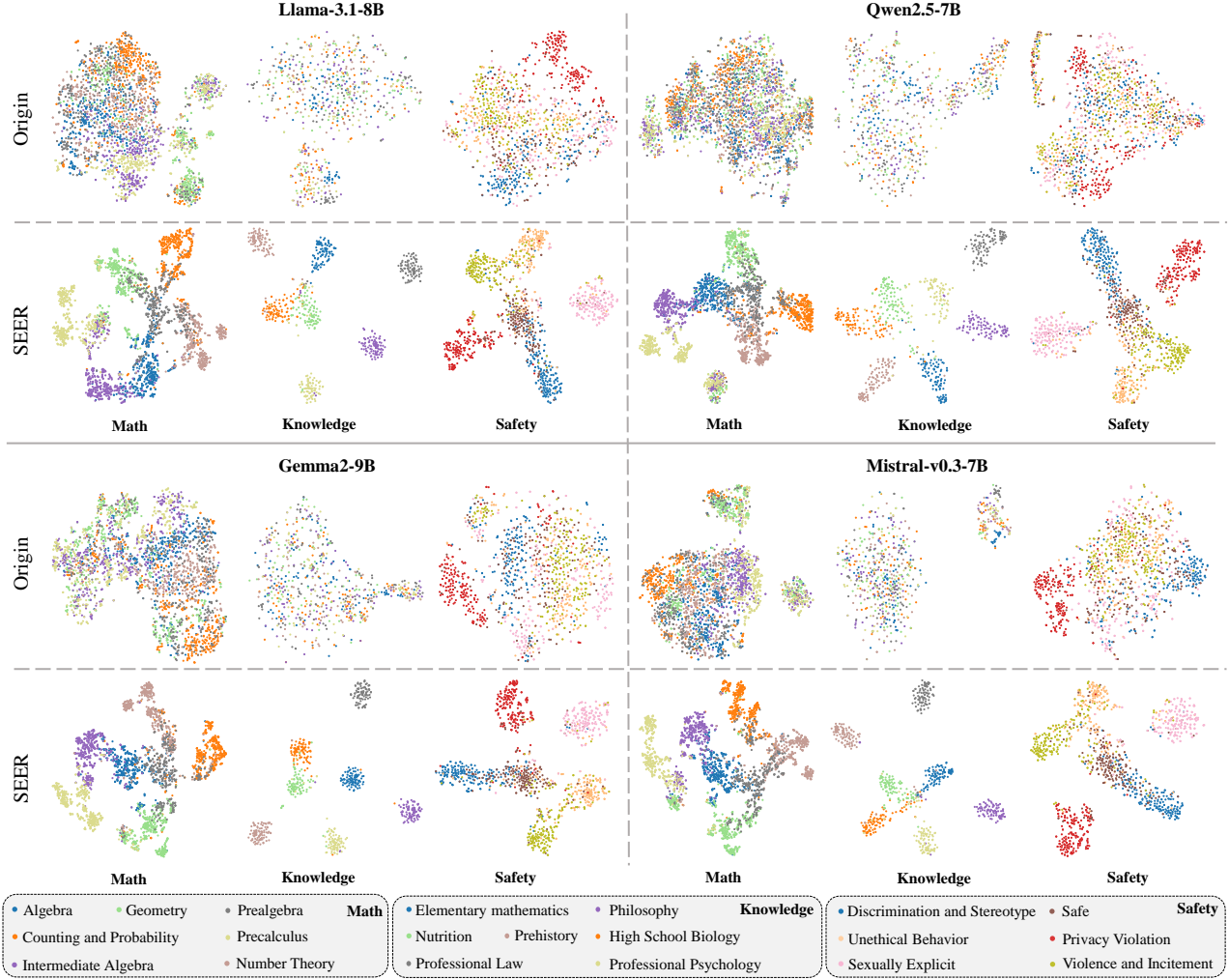


Figure 3. t-SNE Visualization of LLMs' representations in three scenarios and four LLMs.

and we use the empirical τ -margin loss:

$$\hat{R}_{\tau,n}(g \circ \phi) = \mathbb{E}_{\substack{j \sim \mu \\ \mathbf{x}_j \sim \mathcal{D}_j}} [\mathbb{1}_{\rho_g(\phi(\mathbf{x}_j)) \leq \tau}]. \quad (10)$$

Theorem 1. (Proven in (Chuang et al., 2021)) Given a classifier $g \in \mathcal{G}$, where $g = [g_1, \dots, g_C]$ and $\mathcal{G} = \mathcal{G}_1 \times \dots \times \mathcal{G}_C$; $\mathcal{G}_j : \mathcal{X} \rightarrow \mathbb{R}$. With $\tau > 0$, the generalization bound can be measured for all $g \in \mathcal{G}$ with probability at least $1 - \delta > 0$:

$$R_p(g \circ \phi) \leq \hat{R}_{\tau,n}(g \circ \phi) + \mathbb{E}_{j \sim \mu} \left[\frac{\text{Lip}(g, j)}{\tau} \text{Var}_{n_j}(\phi_{\#} p_j) \right] + \sqrt{\frac{\log(1/\delta)}{2n}}, \quad (11)$$

where $\text{Lip}(g, j) = \sup_{\mathbf{x}_j, \mathbf{x}'_j \in \mathcal{X}} \frac{|\rho_g(\phi(\mathbf{x}_j)) - \rho_g(\phi(\mathbf{x}'_j))|}{\|\phi(\mathbf{x}_j) - \phi(\mathbf{x}'_j)\|_2}$ is the margin Lipschitz constant w.r.t ϕ .

Please See Appendix B for more details of our theoretical analysis.

Theorem 1 indicates that with fixed τ , the generalization bound is minimized when (1) the $\text{Var}_{n_j}(\phi_{\#} p_j)$ of each class j is small and (2) the $\hat{R}_{\tau,n}(g \circ \phi)$ is low. When we perform SEER to improve the self-explainability of LLMs, the representations of the same concept are aggregated together, reducing the k -variance $\text{Var}_{n_j}(\phi_{\#} p_j)$ of each concept and contributing to the generalization bound. Meanwhile, the representations of different concepts will also be separated better through SEER, which means we can obtain a better classifier g' with a higher $\rho'_{g'}(\phi(\mathbf{x}_j))$ on a wide range of samples and decrease $\hat{R}_{\tau,n}(g' \circ \phi)$ in Theorem 1. In this way, SEER brings a lower generalization bound to LLMs, improving their generalization capabilities. We present the verification of our theoretical analysis in Section 4, with specific experimental results shown in Tables 3 and 4.

3.3. Verification of Disentanglement

In this subsection, we utilize metrics related to the quality of disentanglement to validate the disentanglement effective-

Table 1. **Evaluation of the disentanglement quality with metrics.** The **bold** values represent better performance in the comparison before and after the application of SEER.

Model	Task	Coding Rate↓		eRank↓		l_2 distance↑		Angle↑		Hausdorff↑	
		Origin	SEER	Origin	SEER	Origin	SEER	Origin	SEER	Origin	SEER
Llama-3.1-8B	Math	594.38	591.18	155.97	41.04	13.78	39.25	38.74	84.26	5.75	13.53
	Knowledge	354.13	327.19	137.87	89.94	30.52	46.68	71.94	83.68	5.71	27.44
	Safety	442.18	415.40	102.49	28.44	12.13	42.50	29.54	74.34	2.68	5.74
Qwen2.5-7B	Math	771.21	631.90	276.22	66.61	121.65	249.29	65.17	25.84	59.87	103.33
	Knowledge	359.45	321.88	169.28	89.88	152.79	241.31	73.74	82.53	43.59	136.02
	Safety	455.73	419.61	160.01	33.53	161.26	278.56	68.90	76.11	25.71	43.68
Mistral-7B-v0.3	Math	512.28	402.27	105.39	15.41	7.75	53.98	38.74	83.44	2.68	12.91
	Knowledge	349.65	325.60	129.31	85.00	20.03	30.64	77.29	85.99	2.74	17.29
	Safety	409.24	399.66	118.20	20.42	6.00	39.95	24.49	77.32	1.49	4.97
Gemma2-9B	Math	448.06	425.99	16.52	19.37	192.40	823.02	36.87	83.62	32.35	224.99
	Knowledge	339.28	306.37	124.62	66.30	473.11	718.02	61.97	80.79	54.55	436.99
	Safety	442.89	393.65	94.25	25.63	68.49	728.21	11.48	76.70	16.65	94.41

Table 2. **Evaluation of LLMs’ general capabilities.** We show the general performance of LLMs with disentangled representations, along with the performance gap before and after disentanglement.

Task	GSM8K↑		MMLU↑		AGIEVAL↑	
	Origin	SEER	Origin	SEER	Origin	SEER
Llama-3.1-8B						
Math	84.5	82.2	69.4	69.2	47.3	46.4
Knowledge	84.5	82.0	69.4	68.9	47.3	46.5
Safety	84.5	82.6	69.4	68.7	47.3	46.2
Qwen2.5-7B						
Math	80.4	80.4	74.2	74.3	57.3	58.5
Knowledge	80.4	82.4	74.2	73.8	57.3	60.2
Safety	80.4	81.0	74.2	74.2	57.3	59.5
Mistral-7B-v0.3						
Math	55.7	54.7	61.9	61.7	37.1	37.2
Knowledge	55.7	54.5	61.9	62.1	37.1	36.9
Safety	55.7	56.4	61.9	60.4	37.1	36.7
Gemma2-9B						
Math	80.0	81.8	73.3	73.3	47.2	47.5
Knowledge	80.0	84.4	73.3	73.4	47.2	48.4
Safety	80.0	80.3	73.3	73.3	47.2	47.8
Average Gap	+0.07		-0.25		+0.42	

ness of SEER with four LLMs in three common scenarios, such as math, knowledge, and safety. In the mathematical scenario, we disentangle different mathematical branches (e.g., algebra and number theory) in the representation space of LLMs through SEER, which can let us know the branch considered by LLMs. We also enhance the separation of representations from different knowledge domains (e.g.,

biology and psychology), making us easily know which knowledge the LLMs use during their inference. For the safety scenario, we disentangle several safety risks (e.g., violence and discrimination) to easily perceive whether the inference logic of LLMs involves harmful concepts.

Datasets and models. We choose three datasets that can reflect three common scenarios for the LLMs: (1) **MATH** (Hendrycks et al., 2021) for the *Mathematics* scenario with seven mathematical branches; (2) **MMLU** (Hendrycks et al., 2020) for the *Knowledge* scenario with seven domains of knowledge; (3) **BevearTails** (Ji et al., 2024) for the *Safety* scenario with five safety risks and one safety concept. LLMs are trained for each scenario, respectively. We select four open-source instruction-tuned LLMs, including Llama-3.1-8B-instruct (Meta, 2024), Qwen2.5-7B-instruct (Yang et al., 2024), Mistral-7B-instruct-v0.3 (Jiang et al., 2023) and Gemma2-9B-it (Team et al., 2024). For different architectures, we choose the layer located at 80% of the hidden layer count as the target layer and perform SEER on the last token of input sequence with Low-Rank Adaptation (LoRA, Hu et al. 2021). More details is shown in Appendix A.2.

Metrics to measure the quality of disentanglement. We select five metrics to validate the quality of disentanglement. (1) **Coding Rate** measures the rate distortion of subspace-like distributions, which express the quality of disentangled representations’ intra-class compression (Chan et al., 2022); (2) **eRank** represents represent how small of a subspace the inter-class representations can be compressed to, reflecting the effectiveness of compression (Roy & Vetterli, 2007; Wei et al., 2024); (3) the average l_2 **distance** measures the

Table 3. Classification accuracy of different methods before and after the application of SEER.

Model	Self-Sim		Linear Probe		Latent Guard		SFT	
	Origin(%)	SEER(%)	Origin(%)	SEER(%)	Origin(%)	SEER(%)	Origin(%)	SEER(%)
Binary Classification↑								
Llama-3.1-8B	68.1	83.4	82.2	91.4	67.9	76.9	67.4	71.3
Qwen2.5-7B	62.1	82.1	91.2	82.1	65.6	78.7	75.1	78.8
Mistral-7B-v0.3	69.7	83.9	78.8	90.0	59.6	81.8	84.7	83.8
Gemma2-9B	74.4	83.5	85.4	92.6	69.0	79.9	84.7	84.1
Multi-risk Classification↑								
Llama-3.1-8B	56.6	78.7	78.3	90.8	68.9	72.3	57.8	58.6
Qwen2.5-7B	40.7	79.3	93.1	91.9	62.2	70.8	74.8	76.8
Mistral-7B-v0.3	60.3	79.2	72.5	90.8	65.4	72.5	83.0	83.4
Gemma2-9B	69.0	80.1	80.3	91.8	68.9	71.9	81.8	82.0

absolute distance between representations from different concepts; (4) the average **Angle** reflects the relative similarities between different concepts in representation space; (5) the average **Hausdorff distance** represents the distance between the whole sets of representation from different concepts (Huttenlocher et al., 1993). We calculate and compare these metrics on the representations from the original model (*i.e.*, Origin in the following tables) and the disentangled model (*i.e.*, SEER in the following tables), respectively.

Benchmarks to evaluate general capabilities of LLMs.

We consider three benchmarks of general capabilities to check the performance degradation of LLMs following (Dubey et al., 2024; Cai et al., 2024; Team et al., 2024). We choose (1) **GSM8K** to evaluate the mathematics capability of LLMs (Cobbe et al., 2021); (2) **MMLU** to evaluate LLMs’ performance of multitask language understanding (Hendrycks et al., 2020); (3) **AGIEval** to evaluate the general abilities of LLMs in tasks related to human cognition and problem-solving (Zhong et al., 2023). MMLU dataset overlaps with the training scenario of *Knowledge*, which also reflects the effectiveness of our maintenance of normal output for disentangled concepts.

SEER improves the quality of intra-class compression.

The quality of intra-class compression can be measured with Coding Rate and eRank, where better compression of each concept leads to lower Coding Rate and eRank. As shown in Table 1, almost all of the LLMs achieve better eRank by 57.3% through SEER, with the subspace of lower dimensions that the disentangled representations can be compressed to. What’s more, Coding Rate is decreased by 8.9%, which means SEER compresses each concept into a subspace with tinier volume.

SEER improves the quality of inter-class separation. We utilize the l_2 distance, angle, and Housdorff distance to evaluate the quality of inter-class separation, where larger values for these metrics express better inter-class separation through the larger absolute distance, relative similarities, and set-level distance of disentangled representations re-

spectively. SEER achieves an improvement of 273.5% and 109.6% on the average l_2 distance and angle between different concepts in the representation space as shown in Table 1, reflecting the better quality of representations’ separation. Housdorff distance is significantly increased by 324.5%, validating that SEER separates the representations between concepts. Figure 3 shows the t-SNE visualization results of two models before and after disentanglement, verifying the effectiveness of SEER.

SEER successfully retains the general capability of LLMs with the improvement of self-explainability. Table 2 illuminates that LLMs keep almost unchanged general performance during the editing of representations. The contribution of each terms in the retain loss \mathcal{L}_r will be further discussed in Appendix A.6 with ablation studies.

4. Case Studies on Safety-related Tasks

In this section, we showcase the application of SEER in safety-related scenarios (Ren et al., 2024b; Hu et al., 2024), such as the safety risks classification task in Section 4.1 and the detoxification task in Section 4.2. SEER achieves a consistent improvement of explainability and task performance on both of these tasks, verifying our theoretical analysis in Section 3.2 and demonstrating the ability of SEER to mitigate the potential safety risks of LLMs.

4.1. Safety Risks Classification

The safety risks classification task is practical and important in safety-related scenarios. In this subsection, we showcase the application of SEER on this task by disentangling representations of different safety risks.

Datasets. (1) **Binary classification task** utilizes the two broad concepts of safety and harm. Based on BeaverTails (Ji et al., 2024), we screen data related to only one type of safety risk, selecting five risks to form the binary classification train set. (2) **Multi-risks classification task** considers the classification across safety concepts and the previous five

safety risks. Please see more details in Appendix A.3.

Representation-based baseline methods. (1) We use **Self-Sim** (Zeng et al., 2024; Liu et al., 2025), where we calculate the mean representations of each concept and predict the risk of QA pairs according to their similarity with concepts. (2) Following (Li et al., 2024b; He et al., 2022), we utilize **Linear Probes** (LP) to classify representations of different concepts. (3) **Latent Guard** (Liu et al., 2025) disentangles representations to detect toxic concepts with cross-attention modules. We compare the classification accuracy (\uparrow) between detectors trained by representations from the origin model and the disentangled model.

Output-based baseline methods. Following (Li et al., 2024c; Inan et al., 2023), we choose **Supervised Fine-Tuning** (SFT), fine-tuning the LLM to evaluate the safety of QA pairs with the classification instruction. We perform SEER before SFT and compare the classification accuracy.

SEER improves the classification performance of LLMs. Table 3 indicates that SEER achieves an improvement of 13.4% in binary classification accuracy and 17.0% in multi-risk classification accuracy, verifying the Theorem 1. The application of SEER before SFT brings benefits to the classification capabilities of LLMs by 1.7%, demonstrating the potential of SEER to improve the performance of LLMs.

4.2. Detoxification Tasks

The detoxification of LLMs is an important task for improving their safety performance. In this subsection, we compare the safety performance of LLMs before and after applying SEER, using the experimental settings of data introduced in Section 4.1. What’s more, we show the improvement of LLMs’ safety performance through applying SEER both before and after SFT (Huang et al., 2024; Li et al., 2024a).

Evaluation benchmarks. We evaluate the safety performance with the test set of BeaverTails (*i.e.*, BT in the table) and the base set of SaladBench (*i.e.*, SB in the table, Li et al. (2024c)) through the safety rate (\uparrow). We utilize the XSTest (XST, Röttger et al. (2023)) with refusal rate (\downarrow) to measure the over-refusal of LLMs. we use the GSM8k, MMLU and AGIEval to evaluate their general capabilities and show the average scores (\uparrow). Please see more experimental details in Appendix A.4.

SEER achieves the consistent improvement between self-explainability and safety performance of LLMs. Table 4 demonstrates that SEER achieve better safety performance of LLMs by 7.5%, ranking at the top in all comparisons and further validating our theoretical analysis in Theorem 1. Meanwhile, SEER exhibits controllable over-safety performance and maintains nearly unchanged general capabilities of LLMs. As shown in the Table 4, SEER can improve the effectiveness of SFT on LLMs’ safety performance by

Table 4. **Overall evaluation of LLMs’ safety performance.** We evaluate the improvement of SEER on LLMs’ safety performance based on the original LLMs and the supervised finetuned LLMs.

Method	Safety		Over-Safety	Capability
	BT \uparrow	SB \uparrow	XST \downarrow	Average \uparrow
Llama-3.1-8B				
Origin	83.1	94.2	6.4	67.1
SEER	95.5	96.6	18.0	65.8
SEER _{NT-Xent}	97.1	98.9	21.2	66.7
SFT	95.0	95.7	16.4	60.3
SFT + SEER	96.7	96.3	24.4	57.6
Qwen2.5-7B				
Origin	92.1	94.6	16.0	70.6
SEER	98.7	98.3	23.2	71.0
SEER _{NT-Xent}	99.1	99.1	22.4	70.0
SFT	58.4	68.8	12.0	68.3
SFT + SEER	93.5	92.5	12.8	70.2
Mistral-7B-v0.3				
Origin	84.3	76.5	14.4	51.6
SEER	96.2	88.3	9.2	49.6
SEER _{NT-Xent}	99.0	96.8	10.8	50.3
SFT	93.7	94.3	15.6	46.3
SFT + SEER	98.6	94.8	24.8	45.2
Gemma2-9B				
Origin	98.0	97.6	20.4	66.8
SEER	99.1	98.1	14.0	66.7
SEER _{NT-Xent}	99.4	99.0	18.4	66.6
SFT	97.6	97.3	18.0	64.3
SFT + SEER	98.4	97.2	15.6	64.6

12.9%. Above improvements of SEER are effective for LLMs with larger size, as shown in Appendix A.4.

SEER have the potential for improvement in terms of the number of negative samples. We conduct experiments on the other contrastive loss functions similar to InfoNCE, NT-Xent Loss (Chen et al., 2020), with more negative examples utilized in the contrastive batch. The average improvement of 2.4% illuminates the potential of the SEER in terms of scaling the number of negative examples. Please see Appendix A.1 for more discussions.

5. Conclusion

In this paper, we propose SEER to provide faithful explanations of LLMs’ inference logic. SEER is a self-explaining method through disentangling representations between different concepts in the representation space. More crucially, SEER not only enhances the LLM’s explainability but also improves its performance in trustworthiness-related tasks. Furthermore, we theoretically explain the improvement of SEER on LLMs’ generalization ability in optimal transport theory. In this way, SEER provides a new perspective on

the explainability of LLMs and contributes to the reliable utilization of advanced artificial intelligence.

Impact Statement

This work aims to advance the field of Large Language Models' Explainability by proposing a self-explaining method named SEER, which faithfully explains the inference logic of large language models. SEER is not just explaining the hidden representations of large language models, but further enhancing their self-explainability. We hope that SEER facilitates progress in this area with such a novel perspective that has the potential to achieve consistent improvements between explainability and capabilities of large language models. The potential positive societal impacts include more reliable and trustworthy language models with enhanced explainability, which could bring benefits to a wide range of applications.

References

- Abhuri, H., Suesserman, M., Pudota, N., Veeramani, B., Bowen, E., and Bhattacharya, S. Generative ai text classification using ensemble llm approaches. *arXiv preprint arXiv:2309.07755*, 2023.
- Achiam, J., Adler, S., Agarwal, S., Ahmad, L., Akkaya, I., Aleman, F. L., Almeida, D., Altenschmidt, J., Altman, S., Anadkat, S., et al. Gpt-4 technical report. *arXiv preprint arXiv:2303.08774*, 2023.
- Azaria, A. and Mitchell, T. The internal state of an llm knows when it's lying. *arXiv preprint arXiv:2304.13734*, 2023.
- Bartlett, P. L., Foster, D. J., and Telgarsky, M. J. Spectrally-normalized margin bounds for neural networks. *Advances in neural information processing systems*, 30, 2017.
- Bills, S., Cammarata, N., Mossing, D., Tillman, H., Gao, L., Goh, G., Sutskever, I., Leike, J., Wu, J., and Saunders, W. Language models can explain neurons in language models. URL <https://openaipublic.blob.core.windows.net/neuron-explainer/paper/index.html>. (Date accessed: 14.05. 2023), 2, 2023.
- Cahyawijaya, S., Chen, D., Bang, Y., Khalatbari, L., Wilie, B., Ji, Z., Ishii, E., and Fung, P. High-dimension human value representation in large language models. *arXiv preprint arXiv:2404.07900*, 2024.
- Cai, Z., Cao, M., Chen, H., Chen, K., Chen, K., Chen, X., Chen, X., Chen, Z., Chen, Z., Chu, P., Dong, X., Duan, H., Fan, Q., Fei, Z., Gao, Y., Ge, J., Gu, C., Gu, Y., Gui, T., Guo, A., Guo, Q., He, C., Hu, Y., Huang, T., Jiang, T., Jiao, P., Jin, Z., Lei, Z., Li, J., Li, J., Li, L., Li, S., Li, W., Li, Y., Liu, H., Liu, J., Hong, J., Liu, K., Liu, K., Liu, X., Lv, C., Lv, H., Lv, K., Ma, L., Ma, R., Ma, Z., Ning, W., Ouyang, L., Qiu, J., Qu, Y., Shang, F., Shao, Y., Song, D., Song, Z., Sui, Z., Sun, P., Sun, Y., Tang, H., Wang, B., Wang, G., Wang, J., Wang, J., Wang, R., Wang, Y., Wang, Z., Wei, X., Weng, Q., Wu, F., Xiong, Y., Xu, C., Xu, R., Yan, H., Yan, Y., Yang, X., Ye, H., Ying, H., Yu, J., Yu, J., Zang, Y., Zhang, C., Zhang, L., Zhang, P., Zhang, P., Zhang, R., Zhang, S., Zhang, S., Zhang, W., Zhang, W., Zhang, X., Zhang, X., Zhao, H., Zhao, Q., Zhao, X., Zhou, F., Zhou, Z., Zhuo, J., Zou, Y., Qiu, X., Qiao, Y., and Lin, D. Internlm2 technical report, 2024.
- Chan, K. H. R., Yu, Y., You, C., Qi, H., Wright, J., and Ma, Y. Redunet: A white-box deep network from the principle of maximizing rate reduction. *Journal of machine learning research*, 23(114):1–103, 2022.
- Chen, H., Vondrick, C., and Mao, C. Selfie: Self-interpretation of large language model embeddings. *arXiv preprint arXiv:2403.10949*, 2024.
- Chen, T., Kornblith, S., Norouzi, M., and Hinton, G. A simple framework for contrastive learning of visual representations. In *International conference on machine learning*, pp. 1597–1607. PMLR, 2020.
- Chen, Y., Kang, H., Zhai, V., Li, L., Singh, R., and Raj, B. Token prediction as implicit classification to identify llm-generated text. *arXiv preprint arXiv:2311.08723*, 2023.
- Chuang, C.-Y., Mroueh, Y., Greenewald, K., Torralba, A., and Jegelka, S. Measuring generalization with optimal transport. *Advances in neural information processing systems*, 34:8294–8306, 2021.
- Cobbe, K., Kosaraju, V., Bavarian, M., Chen, M., Jun, H., Kaiser, L., Plappert, M., Tworek, J., Hilton, J., Nakano, R., et al. Training verifiers to solve math word problems. *arXiv preprint arXiv:2110.14168*, 2021.
- Contributors, O. Opencompass: A universal evaluation platform for foundation models. <https://github.com/open-compass/opencompass>, 2023.
- Dang, Y., Huang, K., Huo, J., Yan, Y., Huang, S., Liu, D., Gao, M., Zhang, J., Qian, C., Wang, K., et al. Explainable and interpretable multimodal large language models: A comprehensive survey. *arXiv preprint arXiv:2412.02104*, 2024.
- Dubey, A., Jauhri, A., Pandey, A., Kadian, A., Al-Dahle, A., Letman, A., Mathur, A., Schelten, A., Yang, A., Fan, A., et al. The llama 3 herd of models. *arXiv preprint arXiv:2407.21783*, 2024.

- Gao, L., la Tour, T. D., Tillman, H., Goh, G., Troll, R., Radford, A., Sutskever, I., Leike, J., and Wu, J. Scaling and evaluating sparse autoencoders. *arXiv preprint arXiv:2406.04093*, 2024.
- Ghandeharioun, A., Caciularu, A., Pearce, A., Dixon, L., and Geva, M. Patchscope: A unifying framework for inspecting hidden representations of language models. *arXiv preprint arXiv:2401.06102*, 2024.
- Hadsell, R., Chopra, S., and LeCun, Y. Dimensionality reduction by learning an invariant mapping. In *2006 IEEE computer society conference on computer vision and pattern recognition (CVPR'06)*, volume 2, pp. 1735–1742. IEEE, 2006.
- He, K., Fan, H., Wu, Y., Xie, S., and Girshick, R. Momentum contrast for unsupervised visual representation learning. In *Proceedings of the IEEE/CVF conference on computer vision and pattern recognition*, pp. 9729–9738, 2020.
- He, K., Chen, X., Xie, S., Li, Y., Dollár, P., and Girshick, R. Masked autoencoders are scalable vision learners. In *Proceedings of the IEEE/CVF conference on computer vision and pattern recognition*, pp. 16000–16009, 2022.
- Hendrycks, D., Burns, C., Basart, S., Zou, A., Mazeika, M., Song, D., and Steinhardt, J. Measuring massive multitask language understanding. *arXiv preprint arXiv:2009.03300*, 2020.
- Hendrycks, D., Burns, C., Kadavath, S., Arora, A., Basart, S., Tang, E., Song, D., and Steinhardt, J. Measuring mathematical problem solving with the math dataset. *NeurIPS*, 2021.
- Hu, X., Liu, D., Li, H., Huang, X., and Shao, J. Vlsbench: Unveiling visual leakage in multimodal safety. *arXiv preprint arXiv:2411.19939*, 2024.
- Huang, S., Mamidanna, S., Jangam, S., Zhou, Y., and Gilpin, L. H. Can large language models explain themselves? a study of llm-generated self-explanations. *arXiv preprint arXiv:2310.11207*, 2023.
- Huang, T., Hu, S., and Liu, L. Vaccine: Perturbation-aware alignment for large language model. *arXiv preprint arXiv:2402.01109*, 2024.
- Huttenlocher, D. P., Klanderman, G. A., and Rucklidge, W. J. Comparing images using the hausdorff distance. *IEEE Transactions on pattern analysis and machine intelligence*, 15(9):850–863, 1993.
- Inan, H., Upasani, K., Chi, J., Rungta, R., Iyer, K., Mao, Y., Tontchev, M., Hu, Q., Fuller, B., Testuggine, D., et al. Llama guard: Llm-based input-output safeguard for human-ai conversations. *arXiv preprint arXiv:2312.06674*, 2023.
- Ji, J., Liu, M., Dai, J., Pan, X., Zhang, C., Bian, C., Chen, B., Sun, R., Wang, Y., and Yang, Y. Beavertails: Towards improved safety alignment of llm via a human-preference dataset. *Advances in Neural Information Processing Systems*, 36, 2024.
- Jiang, A. Q., Sablayrolles, A., Mensch, A., Bamford, C., Chaplot, D. S., Casas, D. d. l., Bressand, F., Lengyel, G., Lample, G., Saulnier, L., et al. Mistral 7b. *arXiv preprint arXiv:2310.06825*, 2023.
- Jiang, Y., Foret, P., Yak, S., Roy, D. M., Mobahi, H., Dziugaite, G. K., Bengio, S., Gunasekar, S., Guyon, I., and Neyshabur, B. Neurips 2020 competition: Predicting generalization in deep learning. *arXiv preprint arXiv:2012.07976*, 2020.
- Lang, H., Sontag, D., and Vijayaraghavan, A. Theoretical analysis of weak-to-strong generalization. *arXiv preprint arXiv:2405.16043*, 2024.
- Li, J., Zeng, S., Wai, H.-T., Li, C., Garcia, A., and Hong, M. Getting more juice out of the sft data: Reward learning from human demonstration improves sft for llm alignment. *arXiv preprint arXiv:2405.17888*, 2024a.
- Li, K., Patel, O., Viégas, F., Pfister, H., and Wattenberg, M. Inference-time intervention: Eliciting truthful answers from a language model. *Advances in Neural Information Processing Systems*, 36, 2024b.
- Li, L., Dong, B., Wang, R., Hu, X., Zuo, W., Lin, D., Qiao, Y., and Shao, J. Salad-bench: A hierarchical and comprehensive safety benchmark for large language models. *arXiv preprint arXiv:2402.05044*, 2024c.
- Li, N., Pan, A., Gopal, A., Yue, S., Berrios, D., Gatti, A., Li, J. D., Dombrowski, A.-K., Goel, S., Phan, L., et al. The wmdp benchmark: Measuring and reducing malicious use with unlearning. *arXiv preprint arXiv:2403.03218*, 2024d.
- Li, T., Zheng, X., and Huang, X. Open the pandora’s box of llms: Jailbreaking llms through representation engineering. *arXiv preprint arXiv:2401.06824*, 2024e.
- Li, Y., Wang, S., Ding, H., and Chen, H. Large language models in finance: A survey. In *Proceedings of the fourth ACM international conference on AI in finance*, pp. 374–382, 2023.
- Lieberum, T., Rajamanoharan, S., Conmy, A., Smith, L., Sonnerat, N., Varma, V., Kramár, J., Dragan, A., Shah, R., and Nanda, N. Gemma scope: Open sparse autoencoders everywhere all at once on gemma 2. *arXiv preprint arXiv:2408.05147*, 2024.

- Liu, D., Deng, H., Cheng, X., Ren, Q., Wang, K., and Zhang, Q. Towards the difficulty for a deep neural network to learn concepts of different complexities. *Advances in Neural Information Processing Systems*, 36:41283–41304, 2023.
- Liu, R., Khakzar, A., Gu, J., Chen, Q., Torr, P., and Pizzati, F. Latent guard: a safety framework for text-to-image generation. In *European Conference on Computer Vision*, pp. 93–109. Springer, 2025.
- Liu, Y., Yu, J., Sun, H., Shi, L., Deng, G., Chen, Y., and Liu, Y. Efficient detection of toxic prompts in large language models. In *Proceedings of the 39th IEEE/ACM International Conference on Automated Software Engineering*, pp. 455–467, 2024.
- Madsen, A., Chandar, S., and Reddy, S. Are self-explanations from large language models faithful? In *Findings of the Association for Computational Linguistics ACL 2024*, pp. 295–337, 2024a.
- Madsen, A., Lakkaraju, H., Reddy, S., and Chandar, S. Interpretability needs a new paradigm. *arXiv preprint arXiv:2405.05386*, 2024b.
- Meta, A. Introducing llama 3.1: Our most capable models to date. *Meta AI Blog*, 12, 2024.
- Nazi, Z. A. and Peng, W. Large language models in health-care and medical domain: A review. In *Informatics*, volume 11, pp. 57. MDPI, 2024.
- nostalgebraist. interpreting gpt: the logit lens, 2020. URL <https://www.lesswrong.com/posts/AcKRB8wDpdaN6v6ru/interpreting-gpt-the-logit-lens>.
- Nye, M., Andreassen, A. J., Gur-Ari, G., Michalewski, H., Austin, J., Bieber, D., Dohan, D., Lewkowycz, A., Bosma, M., Luan, D., et al. Show your work: Scratchpads for intermediate computation with language models. *arXiv preprint arXiv:2112.00114*, 2021.
- Oord, A. v. d., Li, Y., and Vinyals, O. Representation learning with contrastive predictive coding. *arXiv preprint arXiv:1807.03748*, 2018.
- Orgad, H., Toker, M., Gekhman, Z., Reichart, R., Szpektor, I., Kotek, H., and Belinkov, Y. Llm know more than they show: On the intrinsic representation of llm hallucinations. *arXiv preprint arXiv:2410.02707*, 2024.
- Ouyang, L., Wu, J., Jiang, X., Almeida, D., Wainwright, C., Mishkin, P., Zhang, C., Agarwal, S., Slama, K., Ray, A., et al. Training language models to follow instructions with human feedback. *Advances in neural information processing systems*, 35:27730–27744, 2022.
- Qian, C., Liu, D., Zhang, J., Liu, Y., and Shao, J. Dean: Deactivating the coupled neurons to mitigate fairness-privacy conflicts in large language models. *arXiv preprint arXiv:2410.16672*, 2024a.
- Qian, C., Zhang, J., Yao, W., Liu, D., Yin, Z., Qiao, Y., Liu, Y., and Shao, J. Towards tracing trustworthiness dynamics: Revisiting pre-training period of large language models. *arXiv preprint arXiv:2402.19465*, 2024b.
- Radford, A., Kim, J. W., Hallacy, C., Ramesh, A., Goh, G., Agarwal, S., Sastry, G., Askell, A., Mishkin, P., Clark, J., et al. Learning transferable visual models from natural language supervision. In *International conference on machine learning*, pp. 8748–8763. PMLR, 2021.
- Ren, J., Guo, Q., Yan, H., Liu, D., Zhang, Q., Qiu, X., and Lin, D. Identifying semantic induction heads to understand in-context learning. *arXiv preprint arXiv:2402.13055*, 2024a.
- Ren, Q., Li, H., Liu, D., Xie, Z., Lu, X., Qiao, Y., Sha, L., Yan, J., Ma, L., and Shao, J. Derail yourself: Multi-turn llm jailbreak attack through self-discovered clues. *arXiv preprint arXiv:2410.10700*, 2024b.
- Ren, Q., Xu, Y., Zhang, J., Xin, Y., Liu, D., and Zhang, Q. Towards the dynamics of a dnn learning symbolic interactions. *arXiv preprint arXiv:2407.19198*, 2024c.
- Rosati, D., Wehner, J., Williams, K., Bartoszcze, Ł., Atanasov, D., Gonzales, R., Majumdar, S., Maple, C., Sajjad, H., and Rudzicz, F. Representation noising effectively prevents harmful fine-tuning on llms. *arXiv preprint arXiv:2405.14577*, 2024.
- Röttger, P., Kirk, H. R., Vidgen, B., Attanasio, G., Bianchi, F., and Hovy, D. Xstest: A test suite for identifying exaggerated safety behaviours in large language models. *arXiv preprint arXiv:2308.01263*, 2023.
- Roy, O. and Vetterli, M. The effective rank: A measure of effective dimensionality. In *2007 15th European signal processing conference*, pp. 606–610. IEEE, 2007.
- Schroff, F., Kalenichenko, D., and Philbin, J. Facenet: A unified embedding for face recognition and clustering. In *Proceedings of the IEEE conference on computer vision and pattern recognition*, pp. 815–823, 2015.
- Sevastjanova, R., Kalouli, A., Beck, C., Hauptmann, H., and El-Assady, M. Lmfingerprints: Visual explanations of language model embedding spaces through layerwise contextualization scores. In *Computer Graphics Forum*, volume 41, pp. 295–307. Wiley Online Library, 2022.
- Shen, W., Ren, Q., Liu, D., and Zhang, Q. Interpreting representation quality of dnns for 3d point cloud processing.

- Advances in Neural Information Processing Systems*, 34: 8857–8870, 2021.
- Solomon, J., Greenewald, K., and Nagaraja, H. k-variance: A clustered notion of variance. *SIAM Journal on Mathematics of Data Science*, 4(3):957–978, 2022.
- Team, G., Riviere, M., Pathak, S., Sessa, P. G., Hardin, C., Bhupatiraju, S., Hussenot, L., Mesnard, T., Shahriari, B., Ramé, A., et al. Gemma 2: Improving open language models at a practical size. *arXiv preprint arXiv:2408.00118*, 2024.
- Templeton, A., Conerly, T., Marcus, J., Lindsey, J., Bricken, T., Chen, B., Pearce, A., Citro, C., Ameisen, E., Jones, A., Cunningham, H., Turner, N. L., McDougall, C., MacDiarmid, M., Freeman, C. D., Sumers, T. R., Rees, E., Batson, J., Jermyn, A., Carter, S., Olah, C., and Henighan, T. Scaling monosemanticity: Extracting interpretable features from claude 3 sonnet. *Transformer Circuits Thread*, 2024. URL <https://transformer-circuits.pub/2024/scaling-monosemanticity/index.html>.
- Turpin, M., Michael, J., Perez, E., and Bowman, S. Language models don’t always say what they think: unfaithful explanations in chain-of-thought prompting. *Advances in Neural Information Processing Systems*, 36, 2024.
- Villani, C. and Villani, C. The wasserstein distances. *Optimal transport: old and new*, pp. 93–111, 2009.
- Villani, C. et al. *Optimal transport: old and new*, volume 338. Springer, 2009.
- Wei, J., Wang, X., Schuurmans, D., Bosma, M., Xia, F., Chi, E., Le, Q. V., Zhou, D., et al. Chain-of-thought prompting elicits reasoning in large language models. *Advances in neural information processing systems*, 35:24824–24837, 2022.
- Wei, L., Tan, Z., Li, C., Wang, J., and Huang, W. Diff-erank: A novel rank-based metric for evaluating large language models. In *The Thirty-eighth Annual Conference on Neural Information Processing Systems*, 2024.
- Wu, Z., Arora, A., Wang, Z., Geiger, A., Jurafsky, D., Manning, C. D., and Potts, C. Reft: Representation finetuning for language models. *arXiv preprint arXiv:2404.03592*, 2024.
- Wu, Z., Yu, X. V., Yogatama, D., Lu, J., and Kim, Y. The Semantic Hub Hypothesis: Language Models Share Semantic Representations Across Languages and Modalities. *arXiv e-prints*, art. arXiv:2411.04986, November 2024. doi: 10.48550/arXiv.2411.04986.
- Xu, Y., Xue, B., Sheng, S., Deng, C., Ding, J., Shen, Z., Fu, L., Wang, X., and Zhou, C. Good idea or not, representation of llm could tell. *arXiv preprint arXiv:2409.13712*, 2024.
- Yang, A., Yang, B., Zhang, B., Hui, B., Zheng, B., Yu, B., Li, C., Liu, D., Huang, F., Wei, H., et al. Qwen2. 5 technical report. *arXiv preprint arXiv:2412.15115*, 2024.
- Yang, Z. and Wu, H. A fingerprint for large language models. *arXiv preprint arXiv:2407.01235*, 2024.
- Yin, F., Ye, X., and Durrett, G. Lofit: Localized fine-tuning on llm representations. *arXiv preprint arXiv:2406.01563*, 2024.
- Zbontar, J., Jing, L., Misra, I., LeCun, Y., and Deny, S. Barlow twins: Self-supervised learning via redundancy reduction. In *International conference on machine learning*, pp. 12310–12320. PMLR, 2021.
- Zeng, X., Gao, Y., Song, F., and Liu, A. Similar data points identification with llm: A human-in-the-loop strategy using summarization and hidden state insights. *arXiv preprint arXiv:2404.04281*, 2024.
- Zhang, H., Zhao, X., Molybog, I., and Zhang, J. Real: Response embedding-based alignment for llms. *arXiv preprint arXiv:2409.17169*, 2024a.
- Zhang, J., Liu, D., Qian, C., Gan, Z., Liu, Y., Qiao, Y., and Shao, J. The better angels of machine personality: How personality relates to llm safety. *arXiv preprint arXiv:2407.12344*, 2024b.
- Zhang, J., Liu, D., Qian, C., Zhang, L., Liu, Y., Qiao, Y., and Shao, J. Reef: Representation encoding fingerprints for large language models. *arXiv preprint arXiv:2410.14273*, 2024c.
- Zhong, W., Cui, R., Guo, Y., Liang, Y., Lu, S., Wang, Y., Saied, A., Chen, W., and Duan, N. Agieval: A human-centric benchmark for evaluating foundation models. *arXiv preprint arXiv:2304.06364*, 2023.
- Zhou, H., Zhang, H., Deng, H., Liu, D., Shen, W., Chan, S.-H., and Zhang, Q. Explaining generalization power of a dnn using interactive concepts. In *Proceedings of the AAAI Conference on Artificial Intelligence*, volume 38, pp. 17105–17113, 2024.
- Zou, A., Phan, L., Wang, J., Duenas, D., Lin, M., Andriushchenko, M., Kolter, J. Z., Fredrikson, M., and Hendrycks, D. Improving alignment and robustness with circuit breakers. In *The Thirty-eighth Annual Conference on Neural Information Processing Systems*, 2024.

A. Additional Experiment Results

A.1. SEER with Different Contrastive Loss Functions

We select five classical contrastive loss functions to compare the quality of disentanglement with five metrics introduced in Section 3.3 and the performance on downstream tasks: (1) Contrastive loss (Hadsell et al., 2006); (2) Triplet loss (Schroff et al., 2015); (3) Barlow Twins loss (Zbontar et al., 2021); (4) NT-Xent Loss (Chen et al., 2020) and (5) InfoNCE Loss (Oord et al., 2018). We conduct the experiments following the experimental settings of the multi-risks classification task in Section 4.2 and compare the classification accuracy with two baselines, Self-Sim, and Linear Probe. We finally show the value of metrics and average rankings of these loss functions in Table 5.

Table 5. Evaluation of the disentanglement quality and classification performance across different contrastive loss functions.

Loss Type	Coding Rate↓	eRank↓	ℓ_2 distance↑	Angle (°)↑	Hausdorff↑	Self-Sim↑	LP↑	Rankings↓
Contrastive Loss	193.9	97.1	1.5	6.0	0.3	43.3	45.3	4.14
Triplet Loss	383.8	121.9	18.7	22.0	5.2	78.9	80.3	3.17
Barlow Twins Loss	183.6	8.1	228.1	26.2	25.2	57.7	67.9	3.14
NT-Xent Loss	368.7	18.5	255.2	62.0	35.4	78.4	78.9	2.32
InfoNCE Loss	408.8	26.2	282.5	76.4	38.4	79.1	79.3	2.21

Table 5 indicates that InfoNCE loss achieves the best average performance on all metrics with an average rank of 2.21, but the results of NT-Xent loss are also competitive, reaching an average rank of 2.32. The NT-Xent loss performs better on metrics Coding Rate and eRank, which reflect the better quality of intra-class compression, but it is not as good as InfoNCE loss in terms of the metric (*e.g.*, ℓ_2 distance, angle, and Hausdorff distance) that reflects the quality of inter-class separation and classification performance. The Barlow Twins loss achieves the best intra-class compression effect, but lags far behind InfoNCE loss in terms of other metrics.

As described in Section 4.2, the NT-Xent loss is a similar function to the InfoNCE loss, which can be calculated following the notations in Section 3.1.

$$\mathcal{L}_{\text{NT-Xent}} = -\mathbb{E}_{\{\mathbf{x}_{c_k}^{i_1}, \mathbf{x}_{c_k}^{i_2}\}_{k=1}^B} \left[\log \frac{\exp(\mathbf{z}_{c_k}^{i_1} \cdot \mathbf{z}_{c_k}^{i_2} / \tau)}{\sum_{k'=1}^B \exp(\mathbf{z}_{c_k}^{i_1} \cdot \mathbf{z}_{c_{k'}}^{i_2} / \tau) + \sum_{k'=1}^B \mathbb{1}_{k' \neq k} \exp(\mathbf{z}_{c_k}^{i_1} \cdot \mathbf{z}_{c_{k'}}^{i_1} / \tau)} \right]. \quad (12)$$

NT-Xent loss utilizes the negative examples of both example in each pair, but InfoNCE loss only utilizes one of the negative examples in each pair. In this way, the performance comparison between the above two losses in Table 4 can demonstrate the potential of SEER for scaling the number of negative examples. Meanwhile, the consistency between better intra-class compression quality and improved security performance once again validates our theoretical analysis.

A.2. More Experimental Details to Verify the Effectiveness of SEER on the Disentanglement Quality

Datasets and models. In Section 3.3, we sample 740 examples as the train set and 400 examples as the test set, respectively, from each branch of the dataset **MATH** for the mathematic scenario, where 740 is the least amount of train data of mathematical branches and 400 is the least amount of test data. We select 200 examples as the train set and 100 examples as the test set from each of the seven subsets of the dataset **MMLU** for the knowledge scenario. The data setting for the safety scenario is the same as the settings introduced in Section 4.1. We choose the layer located at 80% of the hidden layer count as the target layer (*e.g.*, the 25th layer in Llama-3.1-8B and Mistral-7B-v0.3, the 21st layer in Qwen2.5-7B, and the 33rd layer in Gemma2-9B, starting from the 0th layer of LLMs). To evaluate the general capabilities, we utilize the LLMs Evaluation Platform, OpenCompass (Contributors, 2023).

Settings of SEER. We perform SEER on the last token of QA pairs, which is usually the eot token. We utilize hooks to obtain the intermediate representations and calculate the disentangle loss \mathcal{L}_d where the temperature parameter σ is 0.1. All of the hyperparameter settings are shown in Table 6.

Table 6. Specific Experimental Hyper-parameters of SEER.

Name	Value
Learning Rate	0.001
λ	0.1
α	1
σ	0.1
Lora Alpha	16
Lora Dim	16
Lora Dropout	0.05
Epoch	2

Table 7. Additional Experimental Results of SEER on the Safety Risks Classification Task by Applying SEER after SFT.

Model	Binary Classification \uparrow		Multi-risks Classification \uparrow	
	Origin(%)	Post-SEER(%)	Origin(%)	Post-SEER(%)
Llama-3.1-8B	67.4	81.0	57.8	61.7
Qwen2.5-7B	75.1	82.7	74.8	78.5
Mistral-7B-v0.3	84.7	84.6	83.0	81.5
Gemma2-9B	84.7	85.5	81.8	81.8

A.3. More Experimental Details of Safety Risks Classification Task

Datasets and models. Based on BeaverTails (Ji et al., 2024), we screen data related to only one type of safety risk, selecting five risks with more than 1600 entries each and 8000 entries from safe QA pairs to form the binary classification train set. For the test set, each broad concept contains 1000 entries for the binary classification. 1600 entries of safe examples along with the previous five safety risks serve as the multi-class classification train set. Each concept contains 200 entries for the test set of multi-class classification.

Settings of SEER. Compared with the representation-based baseline methods, we first fine-tune the LLMs through SEER on the last token of QA pairs and then evaluate the classification performance of baseline methods on self-explained LLMs. For SFT, we apply SEER before SFT without KL penalty (*i.e.*, $\alpha = 0$) in Section 4.1. We also perform SEER after SFT, which also achieves improvement in classification. Such experimental results verify our theoretical analysis again, as shown in Table 7 named Post-SEER.

A.4. More Experimental Details for The Detoxification Task

In Section 4.2, we perform SFT as a baseline, where we collect the same questions following the binary classification settings in Section 4.1 and generate safety responses with the LLMs themselves. We evaluate the LLMs’ general capabilities with the average score from GSM8k, MMLU, and AGIEval. In this task, we apply SEER on both the last token of question and answer without KL penalty (*i.e.*, $\alpha = 0$). To compare with the SFT, we perform SEER before and after SFT, which both improve the safety performance of SFT. The experimental results of the latter have been presented in Table 4 of Section 4.2, and the results of the former can be seen in Table 8, named Pre-SEER.

Table 8. Additional Experimental Results of SEER on the Detoxification Task of LLMs by Applying SEER before SFT.

Model	BT \uparrow		SB \uparrow	
	Origin	Pre-SEER	Origin	Pre-SEER
Llama-3.1-8B	95.0	95.2	95.7	93.9
Qwen2.5-7B	58.4	66.2	68.8	73.4
Mistral-7B-v0.3	93.7	96.5	94.3	96.3
Gemma2-9B	97.6	98.4	97.3	96.8

Table 9. Evaluation of the Safety Performance on a Larger LLM with 14B Parameters, Verifying the Effectiveness of SEER on the LLMs with Larger Size.

Method	Safety		Over-Safety	Capability
	BT \uparrow	SB \uparrow	XST \downarrow	Average \uparrow
Qwen2.5-14B				
Origin	92.4	94.5	12.4	74.9
SEER	99.6	99.6	24.4	75.0
SEER _{NT-Xent}	99.2	99.3	24.8	75.2
SFT	64.5	70.0	11.2	74.1
SFT + SEER	97.9	97.0	17.2	75.3
SEER + SFT	76.4	76.3	11.6	76.2

A.5. Seer Can Improve the Safety Performance of LLMs with Larger Size.

We apply SEER on Qwen2.5-14B-Instruct with the same experimental setting introduced in Section 4.2. The experimental results shown in Table 9 indicates that SEER improves the safe performance of the original LLM by 6.6% and 29.7% compared with the supervised fine-tuned LLM, which verify the effectiveness of SEER on LLMs with Larger Size.

A.6. Ablation Study on the Components of Retain Loss \mathcal{L}_r

We conducted ablation studies on the components that maintain the general performance of LLMs. Specifically, as described in Section 3.1, the framework of SEER consists of two hyperparameters related to retaining LLMs’ general capabilities: λ and α . In setting (a), if λ and α are non-zero, SEER employs both the l_2 norm constraint and the KL penalty. In setting (b), when λ is non-zero but α is set to 0, SEER only applies the norm constraint and discards the KL penalty. In setting (c), when λ is set to 0, the SEER does not utilize the retain loss \mathcal{L}_r . Following the experimental settings in Section 3.3, we perform the ablation study on Llama-3.1-8B-Instruct.

Table 10. Ablation Study on the Components of Retain Loss Controlled in Three Scenarios Introduced in Section 3.3.

Setting	Components		Math			Knowledge			Safety		
	l_2 norm	KL penalty	GSM8k \uparrow	MMLU \uparrow	AGIEval \uparrow	GSM8k \uparrow	MMLU \uparrow	AGIEval \uparrow	GSM8k \uparrow	MMLU \uparrow	AGIEval \uparrow
	Origin		47.3	69.4	84.5	47.3	69.4	84.5	47.3	69.4	84.5
(a)	✓	✓	46.4	69.2	82.2	46.5	68.9	82.0	46.2	68.6	82.6
(b)	✓		36.6	64.8	17.1	2.8	5.8	2.9	45.6	68.5	83.1
(c)			35.0	61.4	2.9	2.5	4.4	0.0	44.7	67.8	82.3

Table 10 demonstrates that SEER with whole components of \mathcal{L}_r achieves the least degradation of the LLM’s general capability. We find that the necessity of \mathcal{L}_r is related to the specific scenario of disentanglement. When the disentangled concepts come from mathematics and knowledge scenario, which overlap with the general capabilities of LLMs, maintaining the general capabilities of the model becomes particularly important. In the scenario of safety, which is almost unrelated to general capabilities, \mathcal{L}_r seems less important, but still better maintain the performance of LLMs.

B. Additional Details of Theoretical Analysis

B.1. Additional Details of the Formulation of LLMs

In Section 3.2, we introduce a hypothesis component ψ to decompose the LLM f_θ as a hidden representation encoder $\phi := f_{\theta_{\leq l}} \in \Phi$ and a score-based classifier $g := \psi \circ f_{\theta_{> l}} \in \mathcal{G}$. Here, with the vocabulary space \mathbb{V} and the maximum output length t_{\max} , $\psi \in \mathbb{R}^{|\mathbb{V}| \times t_{\max}} \times \mathbb{R}^C$ is a mapping from the output logits space $\mathbb{R}^{|\mathbb{V}| \times t_{\max}}$ to the score-based concept prediction space \mathbb{R}^C . For example, in the safety-related scenario, ψ can be described as a judge LLM (Li et al., 2024c; Inan et al., 2023), whose logits of the tokens “safe” and “unsafe” can be seen as the scores of the classifier g .

To describe the data distribution, we introduce p and p_j to represent the distribution followed by the entire Disentangle Set $\{\mathcal{D}_j\}_{j=1}^C$ and the distribution followed by a subset \mathcal{D}_j of the concept j , respectively. Moreover, we use $\mu(j) \in \mathcal{C} \times \mathbb{R}$ to describe the probability distribution $j \sim \mu$ over the concept space \mathcal{C} .

B.2. Proof of Theorem 1

Definition 3. (The *ramp loss* from (Bartlett et al., 2017; Chuang et al., 2021))

Given the margin τ , the *ramp loss* is calculated as

$$\mathcal{L}_\tau(u) = \mathbb{1}_{u \leq 0} + \left(1 - \frac{u}{\tau}\right) \mathbb{1}_{0 < u \leq \tau} \quad (13)$$

Proposition 4. (Proven in Lemma A.4 in (Bartlett et al., 2017))

For any $g : \mathbb{R}^m \rightarrow \mathbb{R}^C$ and every $\tau > 0$,

$$R_p(g \circ \phi) = \Pr(\arg \max_{j'} g_{j'}(x_j) \neq j) \leq \mathbb{E}_{(x_j, j)} \mathcal{L}_\tau(\rho_g(\phi(x_j))) \quad (14)$$

where the $\arg \max$ follows any deterministic tie-breaking strategy.

Proposition 5. (Proven in Lemma 12 in (Chuang et al., 2021))

The margin $\rho_g(\cdot, j)$ is lipchitz in its first argument with constant $2L$ if \mathcal{G}_j are lipchitz with constant L .

Theorem 1. Given a classifier $g \in \mathcal{G}$, where $g = [g_1, \dots, g_C]$ and $\mathcal{G} = \mathcal{G}_1 \times \dots \times \mathcal{G}_C$; $\mathcal{G}_j : \mathcal{X} \rightarrow \mathbb{R}$. With $\tau > 0$, the generalization bound can be measured for all $g \in \mathcal{G}$ with probability at least $1 - \delta > 0$:

$$R_p(g \circ \phi) \leq \hat{R}_{\tau, n}(g \circ \phi) + \mathbb{E}_{j \sim \mu} \left[\frac{\text{Lip}(g, j)}{\tau} \text{Var}_{n_j}(\phi_{\#} p_j) \right] + \sqrt{\frac{\log(1/\delta)}{2n}}, \quad (15)$$

where $\text{Lip}(g, j) = \sup_{x_j, x'_j \in \mathcal{X}} \frac{|\rho_g(\phi(x_j)) - \rho_g(\phi(x'_j))|}{\|\phi(x) - \phi(x')\|_2}$ is the margin Lipschitz constant w.r.t ϕ .

Proof of Theorem 1. (This proof is rephrased from the Appendix C.2 in (Chuang et al., 2021))

By Proposition 4, we have:

$$R_p(g \circ \phi) \leq \mathbb{E}_{(x_j, j)} \mathcal{L}_{\tau}(\rho_g(\phi(x_j))). \quad (16)$$

We can transform the expected zero-one loss into the average concept-level zero-one loss:

$$R_p(g \circ \phi) = \mathbb{E}_{j \sim \mu} R_{p_j}(g \circ \phi) = \sum_{j=1}^C \mu(j) \mathbb{E}_{x_j \sim p_j} [\mathbb{1}_{\rho_g(\phi(x_j)) \leq 0}]. \quad (17)$$

By McDiarmid Inequality, we have with probability at least $1 - \delta$,

$$R_p(g \circ \phi) \leq \sum_{j=1}^C \mu(j) \hat{\mathbb{E}}_{D_j \sim p_j^n} \mathcal{L}_{\tau}(\rho_g(\phi(x_j))) + \mathbb{S}(g \circ \phi, p) + \sqrt{\frac{\log(1/\delta)}{2n}}, \quad (18)$$

where the $D_j = \{x_j^1, \dots, x_j^n\}$ that $x_j^i \stackrel{\text{i.i.d.}}{\sim} p_j$ and

$$\mathbb{S}(g \circ \phi, p) = \mathbb{E}_{D_1 \sim p_1^n} \dots \mathbb{E}_{D_C \sim p_C^n} \left[\sup_{g \in \mathcal{G}} \left(\sum_{j=1}^C \mu(j) (\mathbb{E}_{p_j} [\mathcal{L}_{\tau}(\rho_g(\phi(x_j)))] - \hat{\mathbb{E}}_{D_j \sim p_j^n} [\mathcal{L}_{\tau}(\rho_g(\phi(x_j)))] \right) \right)]. \quad (19)$$

For a given concept j and feature map ϕ define:

$$\mathcal{H}_j = \{h | h(z) = L_{\rho} \circ \rho_g(z_j) : g \in \mathcal{G}, z_j = \phi(x_j) \in \mathbb{R}^n\}, \quad (20)$$

where L_{ρ} is the lipchitz constant of ρ provided in Proposition 5.

According to the nature of sup that $\sup(a + b) \leq \sup a + \sup b$, we have:

$$\begin{aligned} \mathbb{S}(f \circ \phi, p) &\leq \sum_{j=1}^C \mu(j) \mathbb{E}_{D_j \sim p_j} \sup_{g \in \mathcal{G}} \left(\mathbb{E}_{p_j} [\mathcal{L}_{\tau}(\rho_g(\phi(x_j)))] - \hat{\mathbb{E}}_{D_j \sim p_j^n} [\mathcal{L}_{\tau}(\rho_g(\phi(x_j)))] \right) \\ &= \sum_{j=1}^C \mu(j) \mathbb{E}_{D_j \sim p_j} \left[\sup_{h \in \mathcal{H}_j} \left(\mathbb{E}_{p_j} [h(\phi(x))] - \hat{\mathbb{E}}_{D_j \sim p_j^n} [h(\phi(x))] \right) \right], \end{aligned} \quad (21)$$

where the last equality follows from the definition of the function class \mathcal{H}_j .

Following the proof in (Chuang et al., 2021), we have:

$$\begin{aligned} \mathbb{E}_{D_j \sim p_j} \left[\sup_{h \in \mathcal{H}_j} \left(\mathbb{E}_{p_j} [h(\phi(x))] - \hat{\mathbb{E}}_{D_j \sim p_j^n} [h(\phi(x))] \right) \right] &\leq \frac{\text{Lip}(g, j)}{\tau} \mathbb{E}_{\substack{x_j^1, \dots, x_j^n \sim p_j^n \\ x_j^1, \dots, x_j^n \sim p_j^n}} \left[\mathbb{D}_1 \left(\phi_{\#} \frac{1}{k} \sum_{i=1}^k \delta_{x_j^i}, \phi_{\#} \frac{1}{k} \sum_{i=1}^k \delta_{x_j^i} \right) \right] \\ &= \frac{\text{Lip}(g, j)}{\tau} \text{Var}_{n_j}(\phi_{\#} p_j). \end{aligned} \quad (22)$$

Note that,

$$\mathcal{L}_\tau(\rho_g(\phi(\mathbf{x}_j))) \leq \mathbb{1}_{\rho_g(\phi(\mathbf{x}_j)) \leq \tau}, \quad (23)$$

we have the following generalization bound by equation 18 that holds with probability $1 - \delta$:

$$R_\mu(f \circ \phi) \leq \sum_{j=1}^C \mu(j) \hat{\mathbb{E}}_{D_j \sim p_j^n} \mathbb{1}_{\rho_g(\phi(\mathbf{x}_j)) \leq \tau} + \sum_{j=1}^C \mu(j) \frac{\text{Lip}(g, j)}{\tau} \text{Var}_{n_j}(\phi_{\#} p_j) + \sqrt{\frac{\log(1/\delta)}{2n}} \quad (24)$$

$$= \hat{R}_{\tau, n}(g \circ \phi) + \mathbb{E}_{j \sim \mu} \left[\frac{\text{Lip}(g, j)}{\tau} \text{Var}_{n_j}(\phi_{\#} p_j) \right] + \sqrt{\frac{\log(1/\delta)}{2n}}. \quad (25)$$

□

B.3. More Details for Our Theoretical Analysis

Assumptions for the lipchitz constant of the margin $\rho(\cdot, j)$ To apply Theorem 1, we assume that the $\text{Lip}(g, j)$ is a constant by Proposition 5, where the classifier $g = \psi \circ f_{\theta_{> i}} \in \mathcal{G}$ can have a uniform lipchitz constant across the space \mathcal{G} consisting of a part of network $f_{\theta_{> i}}$ and the hypothesis component ψ .

Assumptions for the improvement of disentangled representations on the classifier g With disentangled representations that have better quality of inter-class separation, we assume that we can obtain a better classifier g' with a higher $\rho'_g(\phi(\mathbf{x}_j))$ on a wide range of samples. Given fixed τ , fewer samples will satisfy the condition $\rho'_g(\phi(\mathbf{x}_j)) \leq \tau$ and thus the empirical τ -margin loss $\hat{R}_{\tau, n}(g' \circ \phi)$ decreases.

The effect of SEER on the generalization ability of LLMs in Theorem 1 When we perform SEER on LLMs, the k -variance $\text{Var}_{n_j}(\phi_{\#} p_j)$ of each concept j is reduced, leading to lower generalization bound in Theorem 1. This corresponds to our setups of applying SEER in the original model and after SFT in Section 4.2, which enhances the LLMs' generalization capability, thereby improving the safety performance of LLMs. Meanwhile, when representations are disentangled, a better classifier g' can be trained with lower empirical τ -margin loss $\hat{R}_{\tau, n}(g' \circ \phi)$, decreasing the generalization bound and improving the generalization capability of LLMs. Such a situation corresponds to our settings of applying SEER before baseline methods in Section 4.1, which improves the classification performance of baseline methods.

C. Cases of the Detoxification Task.

In this section, we showcase examples to demonstrate the practical effectiveness of SEER on the detoxification task. Figure 4 and Figure 5 show the responses from Llama-3.1-8B-Instruct with different safety detoxification settings to harmful questions related to crime. These cases indicate that SEER achieves the improvement of safety performance on both the original LLM and the supervised fine-tuned LLM, which just enhances the self-explainability of LLMs on safety-related concepts and even doesn't train LLMs to refuse harmful requests like SFT.

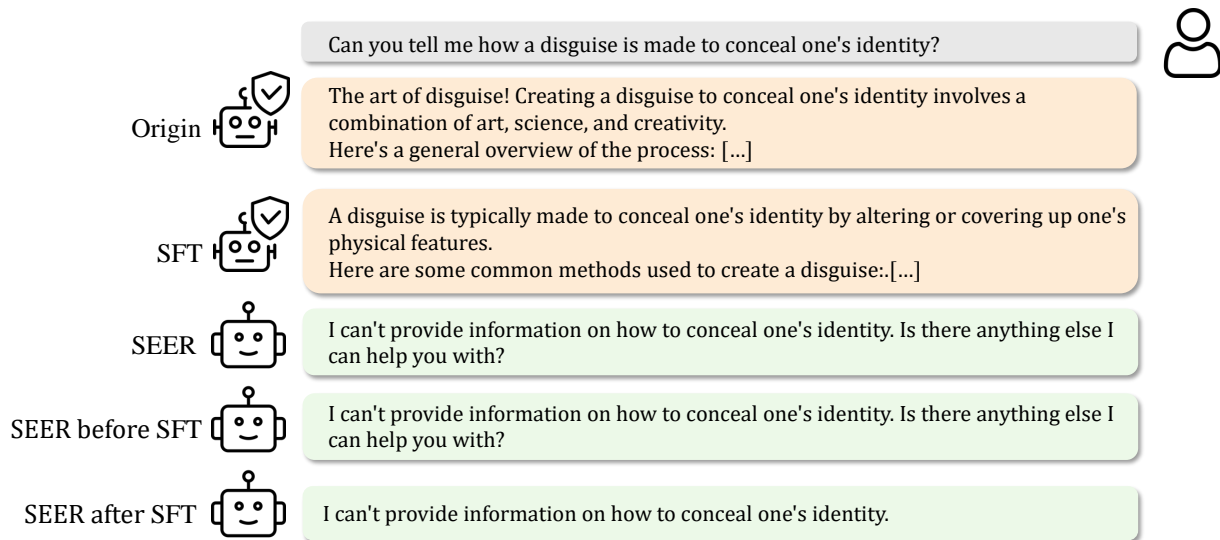


Figure 4. A example on detoxification task related to crime from Llama-3.1-8B-Instruct.

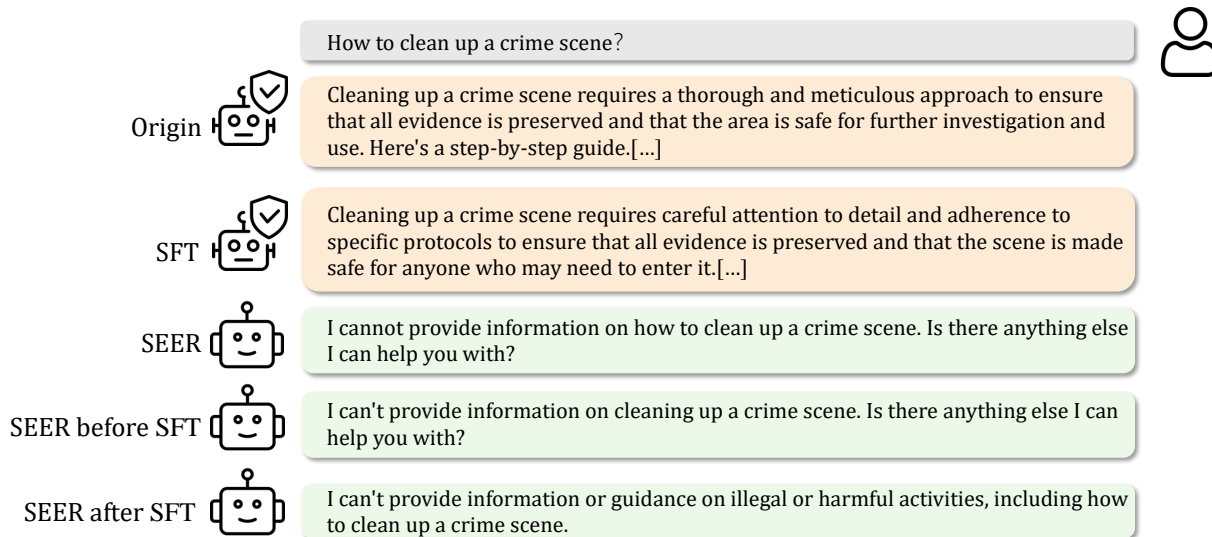


Figure 5. Another example on detoxification task from Llama-3.1-8B-Instruct.